Supporting Information

Volkov et al. 10.1073/pnas.1305821110

SI Materials and Methods

Cloning and Protein Purification. An N-terminal GFP-tagged Dam1 construct was generated by ScaI and AvrII digestion of a pBluescriptII SK(+) plasmid that contained a portion of the Duo1 gene, the Spc34 gene, and an N-terminal fragment of GFP-tagged Dam1; the appropriate fragment was ligated into pC43HSK3H, the polycistronic vector containing the 10 subunits of the Dam1 complex (1, 2), previously digested with ScaI and AvrII. The resulting plasmid was verified by sequencing and then expressed in Rosetta (DE3) -competent cells (EMD Chemicals). WT Dam1 and GFP-Dam1 were purified as described (1) with the following modifications: the lysate was clarified by centrifugation at 30,000 × *g* for 20 min, then loaded onto Ni-nitriloacetic acid agarose (Qiagen), and incubated for 1 h at 4 °C with rocking. The bound protein was eluted with 200 mM imidazole in six 1-mL fractions. Peak fractions were loaded onto a Sephadex G-25 desalting column (GE Life Sciences) and eluted with 20 mM sodium phosphate buffer (pH 6.6) containing 1 mM EDTA and 150 mM NaCl. The resulting protein was applied to a Hi-Trap SP HP 1-mL column (GE Life Sciences), washed with 10 mL same buffer, and then eluted with a linear gradient of 0.15–1 M NaCl. Dam1 usually eluted at 0.3–0.4 M NaCl. The fractions were aliquoted, snap-frozen in liquid N_2, and stored at −80 °C. The coiled coil (CC) tether was generated by fusing GFP binding protein (GBP) and mutant myosin separated by the following linker sequence: DPNSSSVDKLAAALE. GBP-myosin was expressed and purified as in ref. 3. Briefly, the Isopropyl β-D-1-thiogalactopyranoside (IPTG) induction lasted for 2 h; the lysis was performed using the B-PER reagent (Pierce) with 0.1 mg/mL lysozyme and 0.15 M NaCl for 1 h at 4 °C. The Ni-NTA eluate was dialyzed against 1 L 40 mM sodium pyrophosphate (pH 8.5) with 1 mM EDTA and 0.2 M NaCl overnight at 4 °C, then diluted 1:1 with the same buffer containing no added salt, and immediately applied to the 1-mL HiTrap Q HP column. The column was developed with a linear gradient from 0.1–0.5 M NaCl. The peak fractions were dialyzed against 1 L 50 mM sodium phosphate buffer (pH 7.0) with 0.5 M NaCl for 4–12 h at 4 °C, 25% glycerol was added, and then, aliquots were snap-frozen in liquid N_2 and stored at −80 °C.

Measurement of Dam1 Diffusion. To quantify the number of GFP-Dam1 heterodecamers in each fluorescent complex, we compared the intensity of moving dots with the intensity of a single GFP or Alexa488 fluorophore as described (4). Briefly, we recorded the time course of photobleaching for fluorescently labeled Dam1 complexes absorbed to the coverslip surface vs. time (Fig. S3*B*). These values for multiple dots were plotted as a histogram and fitted with equidistant Gaussian distributions (Fig. S3*C*). The distance between Gaussian peaks was taken as the intensity of a single fluorophore. Then, the size of each microtubule (MT) -associated Dam1 complex was determined by measuring its integrated intensity in a circular area 440 nm (6 pixels) in diameter using the first image of the stack to avoid photobleaching. To estimate the number of Dam1 subunits in each complex, these intensities were normalized to the intensity of a single fluorophore. The *x,y* coordinates for each dot were collected manually in MetaMorph (Molecular Devices).

Diffusion coefficients were determined with two methods. First, the squared displacement for each dot was plotted against time, and diffusion coefficients were calculated as one-half the slopes of each track (Fig. S3*D*). The second method was to average the squared displacement at a given time point for all of the dots within the same group of dots of similar size. Weighted linear fitting was applied to these data (Fig. 5*C*), and then, the slopes were divided by two and plotted as diffusion coefficients vs. group size (Fig. 5*D*). The two methods gave similar estimates for Dam1-ring diffusion ($2.5{\cdot}10^{-7}$ and $6.3{\cdot}10^{-7}$ $\mu m^2/s$ for the first and second methods, respectively). Stage drift was determined by observing the position of a fluorescent bead adsorbed to the coverslip. Its diffusion coefficient was determined in the same way as for moving Dam1 spots and used as the lower limit of detectable diffusion. The bond energy for a single Dam1 heterodecamer to MT was estimated from this diffusion coefficient with the help of the mathematical model of Dam1 ring by exponential extrapolation of the theoretical dependency in figure 3a in ref. 5.

The diffusion behavior of differently labeled proteins, GFP-Dam1 and Alexa488-Dam1, was similar. However, the latter protein had to be filtered through a filter column with a 300 kDa cutoff (Pall Corporation) and washed from chambers before imaging to avoid aggregates. GFP-Dam1 showed little aggregation; therefore, both filtered and unfiltered preparations were used, and the data were combined. With Alexa488-Dam1, but not GFP-Dam1, when soluble protein was not removed from the chambers before imaging, we observed some bright, fast-moving, MT-associated complexes. These complexes were unlikely to be rings, because they washed off the MT with a buffer rinse, whereas Dam1 rings form stable MT attachment (4, 6). These Alexa488-Dam1 aggregates seemed to bind to the MTs through interactions with only a subset of their subunits, and therefore, their motions may be similar to the previously described diffusion of charged nanoparticles (7). Similar bright complexes might have previously been interpreted as fast-diffusing Dam1 rings, leading to a discrepancy in past estimates of Dam1 ring diffusion.

Bead Motility Experiments. MTs were nucleated in the presence of 1 mM GTP from purified axonemes using unlabeled tubulin purified from cow brains. Then, the solution was rapidly changed to introduce rhodamine-labeled tubulin in buffer with 0.5 mM Guanosine-5′-[(α,β)-methyleno]triphosphate (GMPCPP). After 7–10 min to allow the elongation of preexisting MTs, all tubulin and nucleotides were washed out. Then, 1–4 nM soluble GFP-Dam1 was added in 80 mM Pipes (pH 6.9) with 4 mM Mg^{2+}, 0.5 mg/mL casein, and 4 mg/mL BSA with strong reducing agent, the conditions identified previously as promoting formation and sliding of a Dam1 ring (4). GFP-Dam1–coated beads were then added, and after the beads attached to the segmented MTs, the MT ends were uncapped by illuminating with either a mercury arc lamp filtered for Texas Red or a 532-nm laser. Images were recorded at 2–3 frames/s, and bead motion was tracked with the MetaMorph software package.

Analysis of Force Signals. Each experiment was recorded at 3 frames/s using differential interferential contrast optics. It was not always possible to visualize the number and direction of the MTs attached to the bead, and therefore, the recordings were analyzed rigorously to avoid false interpretations. For example, in some quadrant photodetector (QPD) recordings, there was more than one rise in amplitude, and in these experiments, we often saw more than red fluorescent cap attached to the bead, suggesting that several MTs became engaged and pulled on the bead sequentially. In this case, the last signal before the bead's complete detachment from the MT was included, and data from preceding phases of motion were discarded. In force-clamp experiments, for each recorded bead, we compared the direction of its motion during

phases III (force clamp) and IV (stationary trap). If these motions were oriented similarly, the recordings were used to determine both the kinetic and force characteristics (see below). However, if the moving bead changed its direction after the force clamp was stopped, only the phase IV data were included in the analysis.

Force signals in a stationary trap were fitted as described previously (8) with the following modifications. The force amplitude was calculated as

$$F = \sqrt{\left(k_x \cdot b_x \cdot e^{-0.5(b_x/r)^2}\right)^2 + \left(k_y \cdot b_y \cdot e^{-0.5\left(b_y/r\right)^2}\right)^2}, \qquad \textbf{[S1]}$$

where r denotes the bead radius, k_x and k_y are trap stiffness values along the coordinate axes of piezo stage, and b_x and b_y are fitted parameters corresponding to maximum bead's displacement from the trap's center. The exponential term $e^{-0.5(b/r)^2}$ was introduced to account for the nonlinearity of the force as a function of the distance from the trap center (9). If the rising part of the signal was interrupted abruptly by the falling part, Eq. **S1** overestimated the force amplitude F; therefore, the following expression was used:

$$F = \sqrt{\left(\left(x_{\max} - x_{final}\right) \cdot k_x \cdot e^{-0.5\left(\frac{x\max - x_{final}}{r}\right)^2}\right)^2 + \left(\left(y_{\max} - y_{final}\right) \cdot k_y \cdot e^{-0.5\left(\frac{y\max - y_{final}}{r}\right)^2}\right)^2}, \qquad \textbf{[S2]}$$

where subscripts *max* and *final* denote the experimentally determined maximal and MT-free bead's displacements along the x and y axes, respectively. The duration of plateau preceding bead detachment was calculated as $p = (t - 2\tau) - (t_1 + 2\tau_1)$, where t and t_1 are the inflection points of the rising and falling portions of the force signal, respectively; τ and τ_1 are 1/4 of the duration of these portions (8).

To analyze the force-clamp results, load acting on the bead as it tracked the MT end in the force clamp was calculated using Eq. **S2**, except the bead's mean displacements during the tracking were used in place of the maximal values. To calculate average tension acting on the beads during repositioning (Fig. 4*D*, red curve), QPD signals for all beads were aligned to center the time of the speed change. Tension values for all beads were averaged at every time point, and the resulting curve was averaged with a running average of 300 time points. The smoothed curve was normalized to the average tension before speed change (Fig. 4*D*). The speed of bead movement under the load was measured from the speed of the stage movement along the MT axis. If speed of the bead's motion increased, only the final speed was used for the force–velocity curves (Fig. 6 *B* and *C*). To obtain force–velocity information from the QPD signals recorded during phase IV (stationary trap), these signals were split into segments with 2- (CC-tethered beads) or 0.5-pN (control beads) force increase, and the average force amplitude during each of these segments was calculated. These segments were then fitted with a linear regression, and the slope was taken as the rate of bead motion. Only the signals in which the bead's movement in force clamp was immediately continued by the movement in the stationary trap at the same speed were included in this analysis (Fig. S2*C* shows an example). These data were combined with the rates and forces obtained during the bead's movement in the force-clamp regime to generate Fig. 5 *B* and C (Fig. S2). Because MT disassembly speed is temperature-dependent (10), all speed values from ref. 11 were multiplied by 1.6 to compensate for the temperature difference (32 °C in our experiments vs. 23 °C in ref. 11).

1. Westermann S, et al. (2005) Formation of a dynamic kinetochore- microtubule interface through assembly of the Dam1 ring complex. *Mol Cell* 17(2):277–290.
2. Miranda JJL, De Wulf P, Sorger PK, Harrison SC (2005) The yeast DASH complex forms closed rings on microtubules. *Nat Struct Mol Biol* 12(2):138–143.
3. Armel TZ, Leinwand LA (2009) Mutations in the beta-myosin rod cause myosin storage myopathy via multiple mechanisms. *Proc Natl Acad Sci USA* 106(15):6291–6296.
4. Grishchuk EL, et al. (2008) Different assemblies of the DAM1 complex follow shortening microtubules by distinct mechanisms. *Proc Natl Acad Sci USA* 105(19):6918–6923.
5. Efremov A, Grishchuk EL, McIntosh JR, Ataullakhanov FI (2007) In search of an optimal ring to couple microtubule depolymerization to processive chromosome motions. *Proc Natl Acad Sci USA* 104(48):19017–19022.
6. Westermann S, et al. (2006) The Dam1 kinetochore ring complex moves processively on depolymerizing microtubule ends. *Nature* 440(7083):565–569.
7. Minoura I, Katayama E, Sekimoto K, Muto E (2010) One-dimensional Brownian motion of charged nanoparticles along microtubules: A model system for weak binding interactions. *Biophys J* 98(8):1589–1597.
8. Grishchuk EL, Molodtsov MI, Ataullakhanov FI, McIntosh JR (2005) Force production by disassembling microtubules. *Nature* 438(7066):384–388.
9. Simmons RM, Finer JT, Chu S, Spudich JA (1996) Quantitative measurements of force and displacement using an optical trap. *Biophys J* 70(4):1813–1822.
10. Fygenson DK, Braun E, Libchaber A (1994) Phase diagram of microtubules. *Phys Rev E Stat Phys Plasmas Fluids Relat Interdiscip Topics* 50(2):1579–1588.
11. Akiyoshi B, et al. (2010) Tension directly stabilizes reconstituted kinetochore-microtubule attachments. *Nature* 468(7323):576–579.

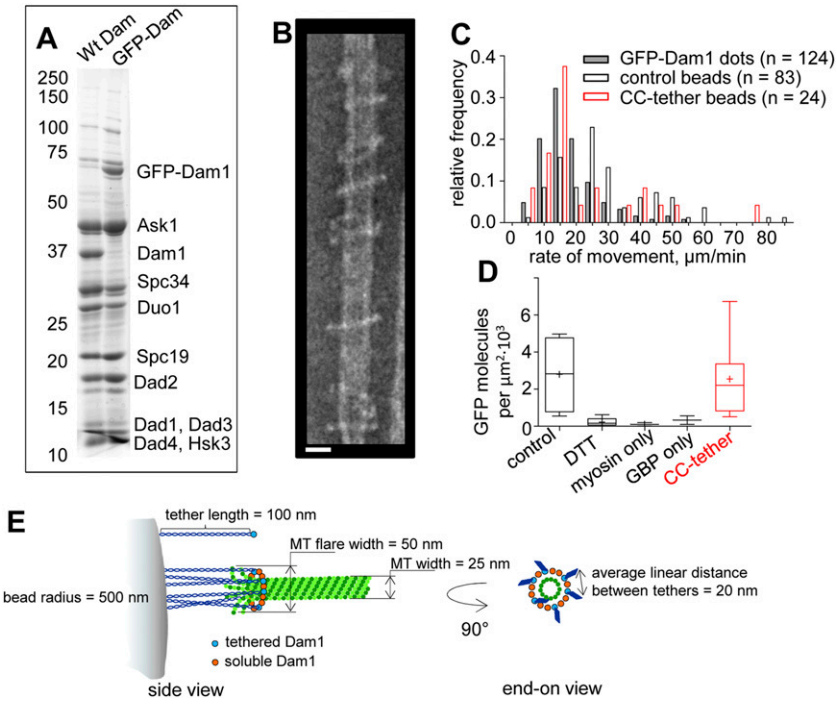

Fig. S1. GFP-Dam1 characterization and bead coating. (*A*) A Coomassie-stained 12% SDS/PAGE of purified WT and GFP-Dam1 complexes; both preparations show near-stoichiometric composition of subunits. (*B*) An electron micrograph of purified GFP-Dam1 mixed with taxol-stabilized MTs and negatively stained shows visibly normal rings. (Scale bar: 25 nm.) (*C*) Motility of soluble Dam1 complexes and Dam1-coated beads with the shortening MTs (*SI Materials and Methods*). (*D*) Fluorescence intensity of the beads coated with GFP-Dam1 by different protocols normalized to the intensity of a single GFP molecule. Three different controls for conjugations are shown, in which a specific step in the bead preparation procedure (*Materials and Methods*) was altered. DTT beads were treated with 10 mM DTT to inactivate maleimide groups before adding myosin-GBP protein. Myosin only beads were incubated with myosin CC with no GBP fusion, whereas GBP only beads were conjugated with purified GBP protein with no myosin CC. These control beads were then incubated with GFP-Dam1 but showed significantly less brightness than the CC-tethered and control beads, testifying to the specificity of conjugation. (*E*) Schematics of an end-on MT attachment to the bead (roughly to scale).

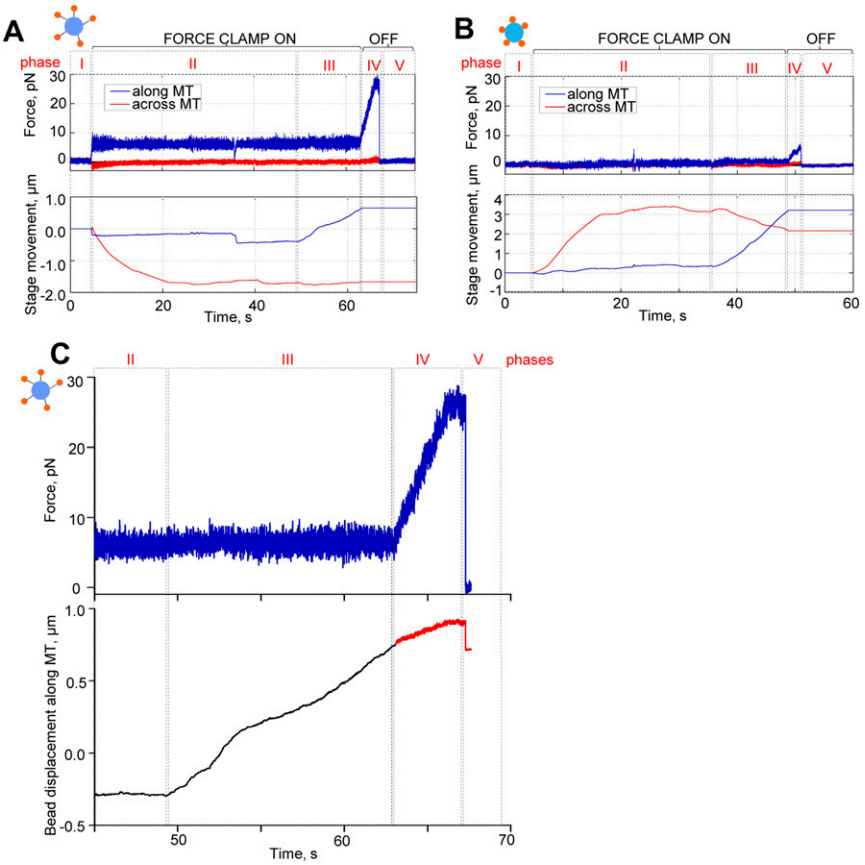

Fig. S2. Analysis of force-clamp data. (*A*) Another example of a force-clamp experiment with a CC-tethered bead (Fig. 4). (*B*) Analogous experiment with a control bead; note the difference in force amplitude for this quadrant photodetector (QPD) signal vs. the signal in *A*. (*C*) Example analysis of the speed of bead motion for the same experiment as in *A* (*Upper*). Black curve in *Lower* shows bead movement along the MT axis during phase III deduced from the stage motions with force clamp on. After the stage stopped moving, the trajectory of bead motion was deduced from the QPD recording (red curve, phase IV). This analysis shows that, after the force clamp was turned off, the bead initially continued to move at the same speed as in phase III, but then, it slowed down; the motion stalled, because the load from the trap increased. The continuity of motion during phases III and IV has enabled us to use the data from both phases to build the force–velocity relationship shown in Fig. 6 *B* and *C*.

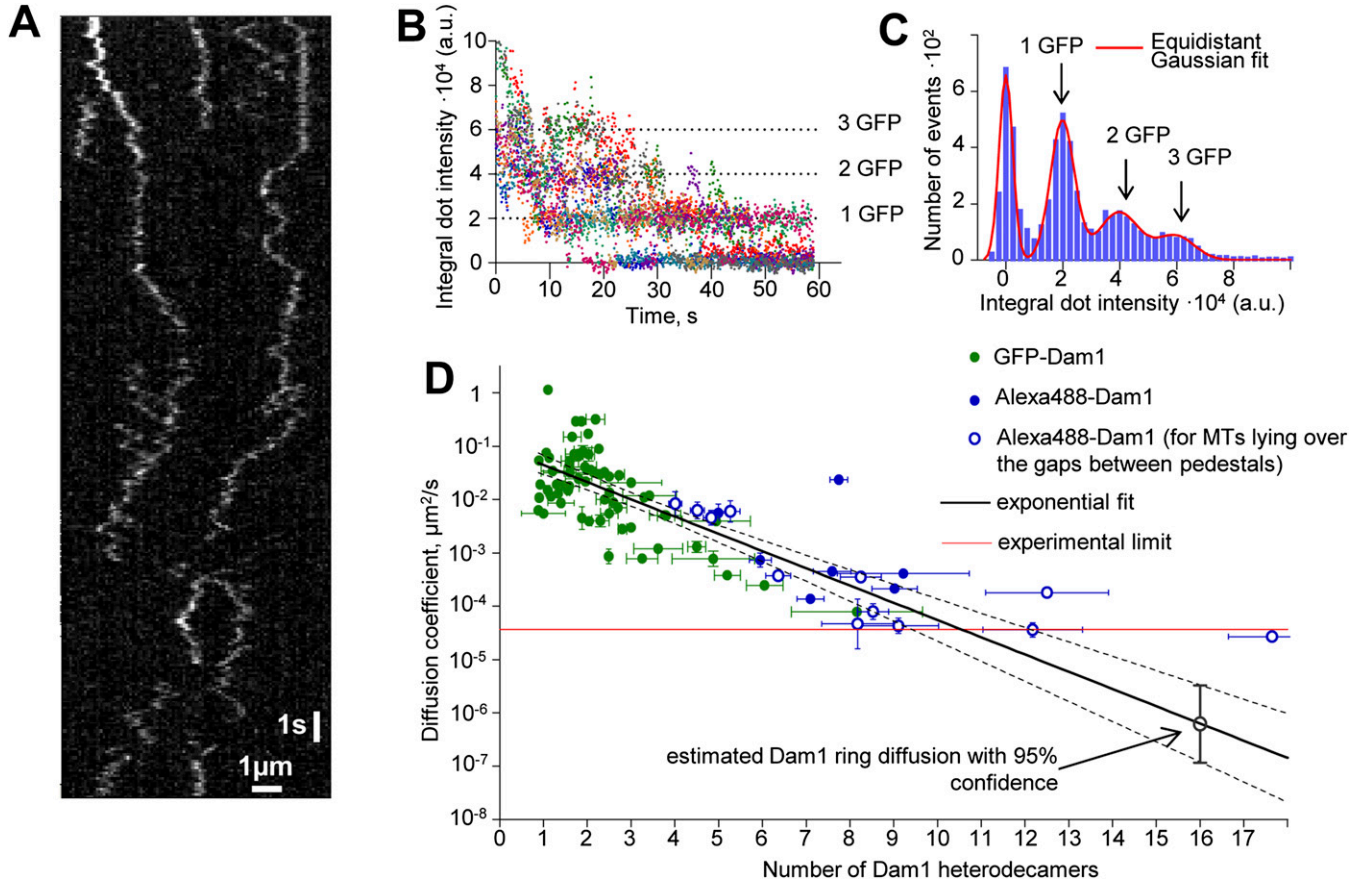

Fig. S3. Diffusion of Dam1 oligomers. (*A*) A representative kymograph for GFP-Dam1 diffusion. To quantify the number of GFP-Dam1 heterodecamers in each fluorescent complex, we compared the intensity of moving dots with the intensity of a single GFP molecule. The latter value was obtained from multiple GFP photobleaching curves, such as shown in *B*, followed by fitting of the resulting intensity histogram with equidistant Gaussian distributions (*C*) (*SI Materials and Methods*). (*D*) Diffusion coefficient vs. oligomer size for individual fluorescent complexes formed by Alexa488-Dam1 (blue) and GFP-Dam1 (green) proteins. The oligomers diffuse along portions of MT suspended between pedestals (open symbols) similarly to those diffusing along coverslip-attached MTs (closed symbols), which was expected for complexes that are small and nonencircling. Black lines are exponential fitting to all data determined by least squares with 95% confidence. The raw data were combined and binned to build a graph on Fig. 5*D*.

Table S1. Parameters for mechanical calculations

Model parameter	Value	Source
MT parameters		
Outer MT diameter	25 nm	1
Wall thickness	5.2 nm	2
Length	1,000 nm	Model parameter
Rigidity modulus	150 pN/nm^2	Calculated based on ref. 3
Protofilament flare parameters		
Number of protofilaments	13	4
Curvature	−0.22 rad	5
Bending stiffness	Varied 9.0–98.3 kcal/(mol rad^2)	Range based on ref. 3
Ring parameters		
Outer diameter	39 nm	6
Thickness	6 nm	7
MT-associated inward linkers	4 nm long, 2 nm thick	7
Linker rigidity	Varied 10^4–10^6 pN/nm^2	Range based on ref. 8
Bead radius	500 nm	Size of experimental beads
Trap stiffness	Varied 0.003–0.03 pN/nm	Experimental range

1. Ledbetter MC, Porter KR (1963) A "microtubule" in plant cell fine structure. *J Cell Biol* 19(1):239–250.
2. Nogales E, Whittaker M, Milligan RA, Downing KH (1999) High-resolution model of the microtubule. *Cell* 96(1):79–88.
3. Molodtsov MI, Grishchuk EL, Efremov AK, McIntosh JR, Ataullakhanov FI (2005) Force production by depolymerizing microtubules: A theoretical study. *Proc Natl Acad Sci USA* 102(12): 4353–4358.
4. Tilney LG, et al. (1973) Microtubules: Evidence for 13 protofilaments. *J Cell Biol* 59(2 Pt 1):267–275.
5. Mandelkow EM, Mandelkow E, Milligan RA (1991) Microtubule dynamics and microtubule caps: A time-resolved cryo-electron microscopy study. *J Cell Biol* 114(5):977–991.
6. Westermann S, et al. (2005) Formation of a dynamic kinetochore- microtubule interface through assembly of the Dam1 ring complex. *Mol Cell* 17(2):277–290.
7. Wang H-W, et al. (2007) Architecture of the Dam1 kinetochore ring complex and implications for microtubule-driven assembly and force-coupling mechanisms. *Nat Struct Mol Biol* 14(8):721–726.
8. Efremov A, Grishchuk EL, McIntosh JR, Ataullakhanov FI (2007) In search of an optimal ring to couple microtubule depolymerization to processive chromosome motions. *Proc Natl Acad Sci USA* 104(48):19017–19022.

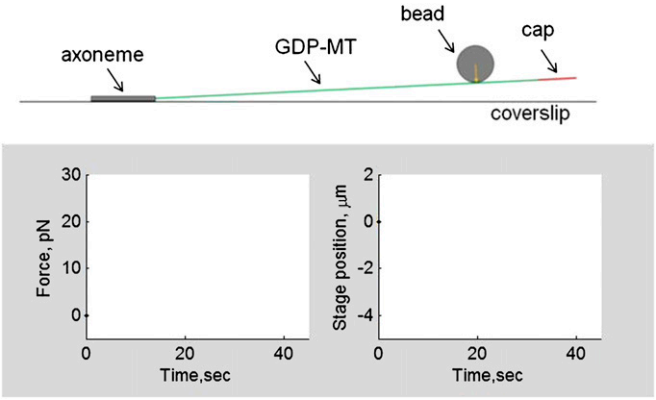

Movie S1. A cartoon illustration of different experimental phases for bead's repositioning from MT lateral to end-on attachment. This movie shows a sequence of events to interpret the experimental traces in Fig. 4*B*.

Movie S1

Movie S2. Diffusion of GFP-Dam1 oligomers along the MT lattice. GFP images of the moving dots on unlabeled and immobilized MTs were recorded continuously with 100-ms exposure. The last image shows the average projection of this stack, and therefore, the MT positions become apparent. A kymograph for the horizontally oriented MT in this movie is shown in Fig. S3*A*. This movie is played two times faster than the frames were taken.

Movie S2